Journal of Sustainability Science and Management
Volume 20 Number 2, February 2025: 297-314
eISSN: 2672-7226
© UMT Press

SYNTHESIS OF GRAPHENE OXIDE FROM SAGO WASTE FOR REMOVAL OF LEAD(II) IONS IN WATER

DAYANG NORAFIZAN AWANG CHEE[1]*, NUR AFIQAH KAMALUDIN[1], LUCY SYLVESTER[1], MUHAMMAD SHAMIL SOFFIAN[1], FAEZRUL ZACKRY ABDUL HALIM[1], CLAUDEAREENA GARLDING[1] AND MOHAMED AFIZAL MOHAMED AMIN[2]

[1]*Faculty of Resource Science and Technology, Universiti Malaysia Sarawak, 94300 Kota Samarahan, Sarawak, Malaysia.*
[2]*Department of Chemical Engineering and Energy Sustainability, Faculty of Engineering, Universiti Malaysia Sarawak, 94300 Kota Samarahan, Sarawak, Malaysia.*

**Corresponding author: dnorafizan@unimas.my*
http://doi.org/10.46754/jssm.2025.02.007
Received: 29 May 2024 Revised: 22 August 2024 Accepted: 6 September 2024 Published: 15 February 2025

Abstract: The goal of this study was to produce Graphene Oxide (GO) from sago hampas for the removal of lead (II) ions in water. The utilisation of sago hampas may promote sustainable practices for GO production using renewable biomass, thus, reducing carbon footprint. The GO was made using a modified Hummers' technique, which resulted in a highly oxidised material with many functional groups. The synthesised GO was characterised using Fourier-Transform Infrared Spectroscopy (FTIR) and Scanning Electron Microscopy (SEM). Batch adsorption tests were performed to evaluate the removal efficiency. The effect of pH, contact time, and initial Pb concentration was investigated during the optimisation process. The outcomes showed that GO had exceptional adsorption capabilities, eliminating over 95% of the Pb at its maximum efficiency. The adsorption kinetics pseudo-second-order model with a regression coefficient of $R^2 = 0.9999$ illustrated a chemical adsorption mechanism. A monolayer adsorption mechanism is suggested by the equilibrium data's good fit to the Langmuir isotherm ($R^2 = 0.9588$). With its large surface area, abundance of functional groups, and strong adsorption affinity, the synthesised GO showed promising properties as an adsorbent for removing Pb from wastewater. This work provides critical knowledge for developing effective and ecologically responsible heavy metal removal adsorbents.

Keywords: Sago hampas, graphene oxide, lead (II) ion, heavy metal, adsorption.

UNCORRECTED PROOF

Introduction

Increasing global water contamination requires regular evaluation of responsible and ecologically responsible management approaches. The 2030 Agenda, through Goal 6 of the Sustainable Development Goals aims to ensure sustainable water and sanitation for all by 2030 (UNEP, 2020). Access to clean water, sanitation, and hygiene is vital for health, education, and poverty reduction. Toxic heavy metals from industries such as mining, automobiles, and agriculture are particularly concerning. These non-biodegradable and carcinogenic metals can severely impact one's health (Qasem *et al*., 2021). High levels of metals like mercury (Hg) and lead (Pb) can cause kidney failure, stomach pains, and bloody diarrhoea (Balali-Mood *et al*., 2021). Lead is highly toxic and can damage organs through immune modulation, oxidative stress, and inflammation.

Therefore, various techniques exist for heavy metal removal, including membrane processes, ion exchange, chemical precipitation, and adsorption. However, in this study, adsorption was chosen as it is very promising due to its cost-effectiveness and environmental friendliness (Luo *et al*., 2020).

Graphene-based adsorbents, particularly Graphene Oxide (GO), a two-dimensional (2D) material are very popular due to their high surface-to-volume ratio and abundant oxygenated-functional groups (hydroxyl,

carbonyl, carboxyl, and epoxy groups). These groups enhance its hydrophilicity in aqueous solutions and provide reactive sites for covalent bonding, dipole-dipole interactions, or electrostatic interactions with the adsorbate (Ahmad *et al*., 2020). Furthermore, this GO is excellent for removing heavy metal ions due to its well-ordered structure, high specific surface area, and versatile surface functionalisation options. Additionally, GO can be derived from biomass sources or waste materials, enhancing its sustainability. However, achieving an economical and efficient synthesis of GO remains a challenge (Yu *et al*., 2016).

Sarawak, which is the largest exporter of sago, produces a significant amount of waste. Transforming this sago waste into high-value products can effectively tackle environmental concerns and promote sustainable resource utilisation. The lignocellulosic matrix of sago waste, rich in carbon neutrality, makes it an excellent feedstock for various industrial applications. This not only helps mitigate environmental issues but also contributes to addressing the impending fuel shortage crisis (Amin *et al*., 2019). As a result, the use of graphene oxide derived from sago waste for lead adsorption offers a promising solution for water contamination.

Therefore, in this study, GO extracted from sago hampas waste was chemically synthesised using a modified Hummers' technique. The morphology and characteristics of GO were identified using FTIR and SEM spectroscopy. The adsorption ability of GO towards Pb(II) was determined via batch adsorption test to determine the adsorption kinetics and isotherms of the adsorption. The impact of pH, contact time, and initial Pb concentration was investigated during the optimisation process. To date, no study has investigated the application of GO membrane on support to remove Pb(II). Therefore, the present study was conducted to synthesise, characterise, and determine the potential GO for the removal of Pb(II) in the aqueous environment.

Materials and Methods

Pretreatment of Sago Waste

Sago hampas is a starchy lignocellulosic biomass produced during the extraction of sago starch, which contains 58% starch, 23% cellulose, 9.2% hemicellulose, and 3.9% lignin. The sago hampas were obtained from Mukah, Sarawak and underwent a pretreatment process. Initially, the sago was washed, cleaned, and dried in an oven at 60°C for two days. After drying, the sample was crushed into granular particles with a size of 2 to 3 mm. The crushed sample was then carbonised at around 400°C for five hours to yield highly carbon sago waste charcoal. This charcoal was subsequently ground and sieved using 200 mesh to obtain particles sized 75 μm. The pretreated sago waste was then used to synthesise graphite powder.

Synthesis of Graphite Powder from Sago Waste

About 40% hydrofluoric acid (*HF*) was used to wash the sample. This was to prevent any impurities and compound presence. The sample containing the HF was agitated for three hours at 45°C with a sample-to-acid ratio of 1:3. The solution was then dried in an oven at 110°C for 12 hours after being rinsed with deionised water and *NaOH* to a pH of 6 to 7. The phase composition of the sample was determined by characterising the resulting graphite powder using FTIR and SEM (Sujiono *et al*., 2020).

Preparation of GO from Graphite Oxide

The modified Hummers method was used to prepare GO (Sujiono *et al*., 2020). Graphite from sago (1 g) and $NaNO_3$ (0.5 g) was added to 25 mL of H_2SO_4 before being agitated for 30 minutes in an ice bath. Following the stirring, 3 g of $KMnO_4$ was gradually added to the mixture and the mixture was stirred for another three hours until its colour changed. In an ice bath, the temperature was held between 20°C and 10°C throughout the stirring operation. Following the removal of the solution from the ice bath, stirring

UNCORRECTED PROOF

was carried out continuously for an additional hour at a temperature of 35°C. The solution was then agitated for one hour after receiving a gentle addition of deionised water (50 mL). Following that, 100 mL of deionised water was added and sterilised for one hour. The solution was sterilised for 30 minutes to eliminate any extra $KMnO_4$ before receiving a gradual addition of hydrogen peroxide (H_2O_2) (5 mL). Vacuum pump filtration was used to separate the precipitate from the liquid and deionised water was added until the pH is neutral. The precipitate was dried in an oven for 12 hours at 110°C to create GO powder.

Characterisation of ZIF-8 and Its Modification

FTIR and SEM were used to characterise the obtained GO from sago hampas. The functional groups of the GO were identified using KBr pellets and an FTIR device from Thermo Scientific called the Nicolet iS10. FTIR spectroscopy was conducted on raw sago, Commercial Graphite Oxide (CGTO), Synthesised Graphite Oxide (SGO), and GO using a Thermo Scientific Nicolet iS10 instrument and KBr pellets in the 4,000 to 5,000 cm^{-1} range to detect their functional groups. A graph displaying the peak interactions of each molecule in the sample and their absorption of energy from the infrared region of the electromagnetic spectrum present the findings of the FTIR spectroscopy observations.

Scanning Electron Microscopy (SEM) characterisation of the GO's surface morphology and elemental composition was also done. The SEM produces high-resolution images by scanning a focused electron beam across the surface of the subject. This makes it possible to see the material's shape, topography, and structural characteristics.

Adsorption of Pb(II) Experiment

Batch adsorption experiments were conducted to investigate the adsorption of Pb(II) ions onto graphene oxide in different pH ranges – 4, 6, and 8, contact time – one to six hours, and different initial concentrations of Pb(II) at 20, 40, 60, 80, and 100 ppm. In each experiment, 0.020 g of GO was immersed in a 50 mL solution containing Pb(II) ions at different pH. The samples were agitated at 250 rpm for 15 hours at ambient temperature. Atomic Absorption Spectroscopy (AAS) was used to measure the concentration of metal ions. The percentage of Pb(II) removal was calculated using Equation 1 and the adsorption capacity of GO was determined using Equation 2.

The initial concentration was set at 20 ppm, as it is the minimum concentration commonly selected by researchers to evaluate removal efficiency. The contact time was set between 1 and 6 hours to determine the optimal duration required for the complete removal of Pb(II). The chosen pH range of 4 to 7 was selected based on the findings of Nguyen *et al*. (2021), who showed that Pb(II) removal is maximised within this range. Additionally, a pH of 8 was included to observe whether an acidic condition affects the adsorption capacity.

$$\text{Pb (II) removal (\%)} = \frac{Co - Ce}{Ce} \text{ x } 100 \quad (1)$$

$$\text{qe} = \frac{Co - Ce}{m} \text{ x } V \quad (2)$$

where:

C_o (mg/L) = Pb(II) Ion Initial Concentration; C_e (mg/L) = Pb(II) Ion Final Concentration; m (mg) = Adsorbent Mass; V (L) = Pb(II) Solution Volume

Analysis Models for Pb(II) Batch Adsorption Test

Adsorption Isotherm Models

As the adsorption process approaches equilibrium, adsorption isotherms provide valuable insights into the interactions between adsorptive molecules and adsorbents. This help in understanding how these molecules distribute between the solid and liquid phases. Therefore, maximising the adsorbent for the selective eradication of environmental pollutants is essential. The isotherm data are fitted with various models for this investigation (Khurana *et al*., 2018).

UNCORRECTED PROOF

Under conditions of constant temperature, the adsorbed solute's equilibrium state and its concentration in solution are correlated by the adsorption isotherm. Freundlich and Langmuir's isotherms typically explain the distribution pattern of metal ions. The Freundlich isotherm presupposes that heterogeneous surfaces are used for the adsorption process. In contrast, the Langmuir isotherm assumes the adsorption occurs on a homogeneous adsorbent surface with the adsorbate covered in a monolayer (Awang Chee *et al*., 2021). The Langmuir and Freundlich isotherm model is expressed in Equations 3 and 4, respectively as below:

$$\frac{C_e}{q_e} = \left(\frac{1}{q_m}\right)C_e + \frac{1}{q_m K_L} \quad (3)$$

$$\log q_e = \log K_F + \frac{1}{n}\log C_e \quad (4)$$

Kinetic Isotherm Models

In this study, the kinetics of Pb(II) adsorption onto GO were evaluated using various kinetic models. The mechanisms of adsorption were investigated through different equations, including the well-known models, which were Pseudo-First-Order and Pseudo-Second-Order, to study the adsorption rate of the Pb(II) removal. The experimental data and the value predicted by the model agreed, according to the correlation coefficient (R2). The formula for each Pseudo-First-Order (Equation 5) and Pseudo-Second-Order (Equation 6) model that was used to analyse the rate of this adsorption study is shown below:

$$log\,(q_e - q_t) = log\,q_e - k_1 t \quad (5)$$

where t denotes the amount of metal ion adsorbed at time t (min), k_1 (min^{-1}) is the Pseudo-constant for the first order, and q_e denotes the theoretical equilibrium adsorption capacity (mg/g). The equation for Pseudo-Second-Order:

$$\frac{t}{q_t} = \left(\frac{1}{q_e}\right)t + \frac{1}{k_2 q_{e^2}} \quad (6)$$

where k_2 is the Pseudo-Second-Order rate constant ($g.mg^{-1}.g^{-1}$) and t is the metal ion adsorbed (min), respectively.

Results and Discussion

SEM Analysis

Figure 1 shows the surface morphology of raw sago hampas waste at magnifications of 500x (50 m size bar) and 5,000x (5 m size bar). When examined using a scanning electron microscope, untreated sago hampas waste typically exhibits a surface texture characterised by fibrous and granular features. When viewed under a scanning electron microscope, raw sago hampas waste shows a rough and uneven surface. The fibres in the waste are irregular in shape and thickness; the surface has noticeable cracks and gaps.

The material contains starch granules and other plant parts, giving it a granular texture.

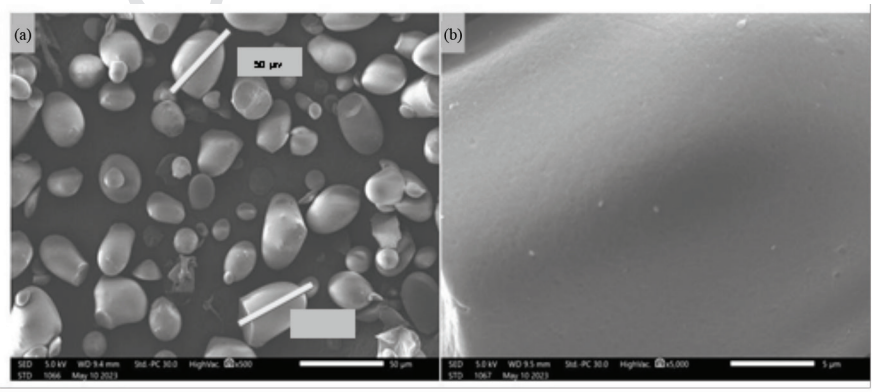


Figure 1: SEM image of the raw sago hampas waste, (a) with magnification 500× and (b) 5,000×

UNCORRECTED PROOF

The SEM images reveal a network of fibres that are interwoven and the oval-shaped starch granules, which sometimes have flat edges are visible. These granules are about 20 to 60 µm in size, adding to the detailed picture of the sago hampas waste.

The surface morphology of commercial graphite oxide is depicted in Figure 2 at magnifications of 2,000× (10 µm size bar), 5,000× (10 µm size bar), 10,000× (5 µm size bar), and 20,000× (1 µm size bar). Under a scanning electron microscope, graphite oxide exhibits a layered and wavy surface appearance. When it comes to the way graphite layers are stacked, the individual graphene oxide sheets are arranged in a layered pattern. These layers can give the surface a particular texture by appearing wrinkled, folded, or twisted. Commercial graphite often consists of natural or manufactured graphite flakes. When examined under a scanning electron microscope, these flakes typically appear as flat, plate-like structures with smooth surfaces. The edges of the flakes can be irregular and jagged.

The size and thickness of the flakes can vary depending on the graphite's grade and quality. In addition to these flakes, commercial graphite may also feature granular structures. These granules often form when impurities or other carbon-based materials mix with graphite. As a result, the granules can differ in size, shape, and composition, leading to a diverse and irregular appearance in SEM images.

Additionally, the surface morphology of SGtO can be seen in Figure 3 at 1,000x (10 µm size bar), 2,000x (10 µm size bar), and 5,000x (5 µm size bar) magnifications. Compared with the commercial graphite obtained in the store, the synthesised graphite has a slightly clearer morphology than the CGtO. Graphite produced synthetically can take the form of flake shapes as well as granular structures. These granules are frequently created when graphite is combined with impurities or other carbonaceous substances.

The GO sample as shown in Figures 4 (a) and (b) has particles with sizes ranging from 5 µm to 10 µm, whereas Figures 4 (c) and (d) for the GO sample show particle size in 1 µm. The GO sample surface is densely packed with granular particles and has pores of various sizes.

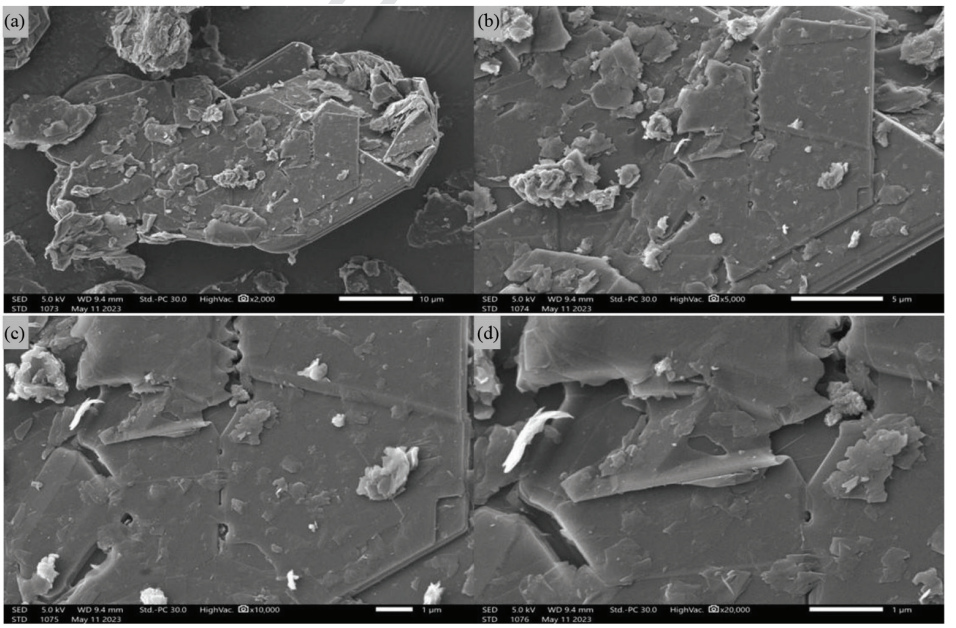


Figure 2: SEM image of the CGtO samples, with magnification (a) 2,000×, (b) 5,000×, (c) 10,000×, and (d) 20,000×

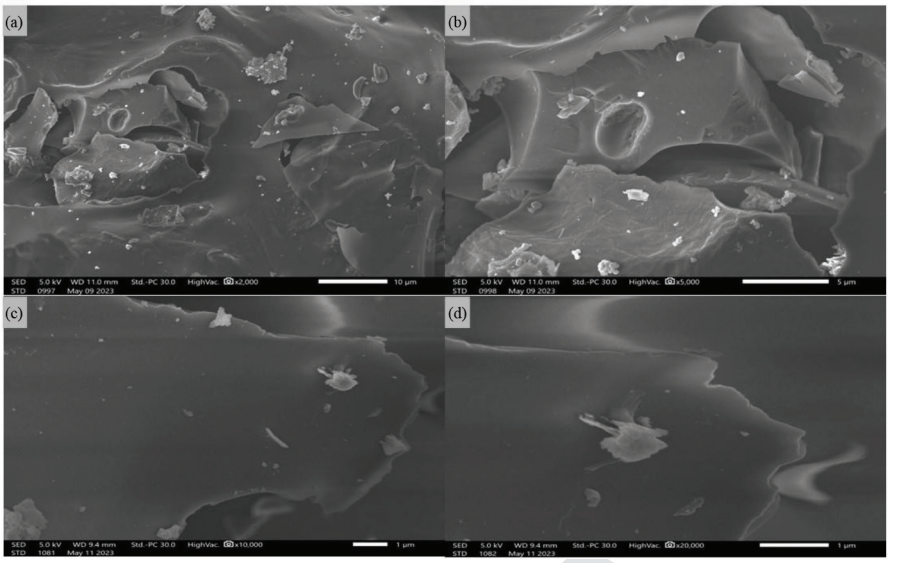


Figure 3: SEM image of the SGtO samples based on sago hampas waste, (a) with magnification 2,000×, (b) 5,000×, (c) 10,000×, and (d) 20,000×

The GO sheets that are partially separated or overlapped may be visible in the SEM pictures, creating a rough and uneven surface. The surface may also have minor flaws like cracks or holes, as well as oxygen-containing functional groups, which might show up as tiny protrusions or contrast fluctuations. The GO sheets obtained by sonication of graphite oxide exhibit distinct characteristics, as described by Shojaeenezhad *et al*. (2017). These sheets are thin, flexible, and display a wrinkled morphology.

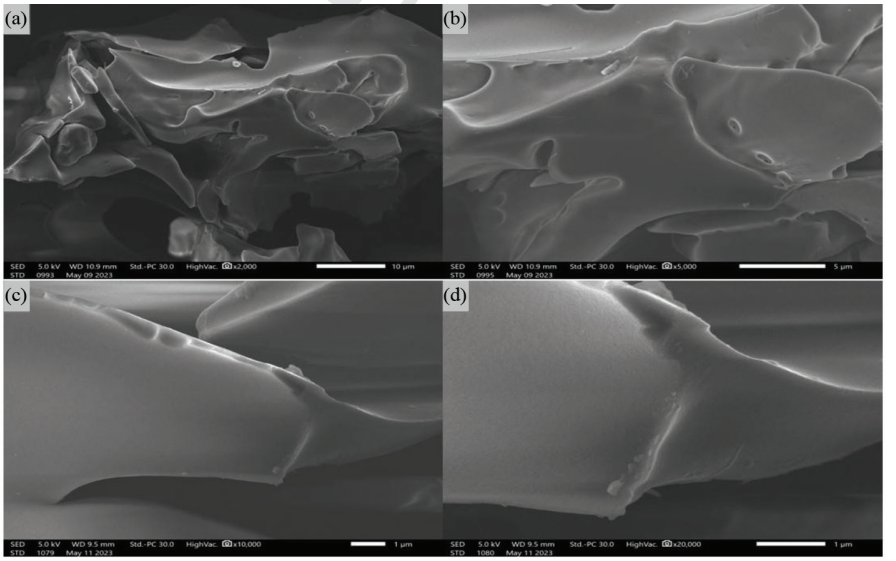


Figure 4: SEM image of the GO samples based on sago hampas waste, (a) with magnification 2,000×, (b) 5,000×, (c) 10,000×, and (d) 20,000×

FTIR Analysis

The locations of the absorption peaks in the FTIR spectrum of raw sago are shown in Figure 5 (a), which represents differences in bond energy between various functional groups. The stretching vibrations of the hydroxyl groups (-OH) in water molecules are 3,450.06 cm^{-1} wavenumbers peak. Alkane (-CH) vibrations cause peaks at 2,944.62 cm^{-1} to appear. The peak at 1,142.06 cm^{-1} corresponds to tertiary alcohol (C-OH) vibrations while the peak at 1,642.77 cm^{-1} indicates the vibration of alkane stretching (C-=C) groups. The peak at 773.42 cm^{-1} represents the bending vibrations of alkene (C=C) groups.

Bohari *et al*. (2020) explained that the sago pith biochar's C-H extending between 2,840 and 3,000 cm^{-1} confirms the presence of alkane groups. Sago pith biochar included conjugated aldehydes, as evidenced by the peak's C=O stretching (1,685-1,710 cm^{-1}). All the biochars showed evidence of C-H stretching, aromatic C=C stretching, and C=O stretching, per the study of their FTIR spectra. This finding shows that cellulose, hemicelluloses, and lignin may have degraded and depolymerised as the temperature rise during the carbonisation of the biochar (Bohari *et al*., 2020).

Figure 5 (b) illustrates the positions of the absorption peaks in the FTIR spectrum of CGtO as a reference to the synthesised graphite oxide powder. There are indicating variations in bond energy across different functional groups. The peak wavenumber of the stretching vibrations exhibited by the hydroxyl groups (-OH) present in water molecules is 3,439.00 cm^{-1}. The presence of alkene (-C=C) vibrations results in the emergence of peaks at a wavenumber of 1,624.34 cm^{-1}. The peak observed at 1,116.85 cm^{-1} is attributed to the secondary alcohol (C-OH) vibrations, whereas the peak at 612.81 cm^{-1} is indicative of the vibration of the halo compound (C-Br).

Figure 6 depicts the positions of absorption peaks in the FTIR spectrum of the SGtO powder. These peaks highlight variations in bond energy among different functional groups. Specifically, the stretching vibrations of hydroxyl groups (-OH) present are observed at a wavenumber of 3,449.51 cm^{-1}. Peaks at 1,612.60 cm^{-1} correspond to stretching alkene (-C=C) vibrations. Furthermore, the peak at 1,120.52 cm^{-1} is attributed to secondary alcohol (C-OH) vibrations while the peak at 747.90 cm^{-1}indicates the bending vibration of alkene (C=C). FTIR results of SgtO are almost identical to the CGtO as the reference.

The positions of absorption peaks in the FTIR spectrum of GO are illustrated in Figure 7 (a). The observed peaks serve to underscore the discrepancies in bond energy that exist between distinct functional groups. The stretching vibrations of hydroxyl groups (-OH) that are inherent are detected at a specific wavenumber of 3,458.80 cm^{-1}. The vibrational peaks observed at 1,630.56 cm^{-1} are indicative of stretching alkene (-C=C) vibrations. The peak observed at

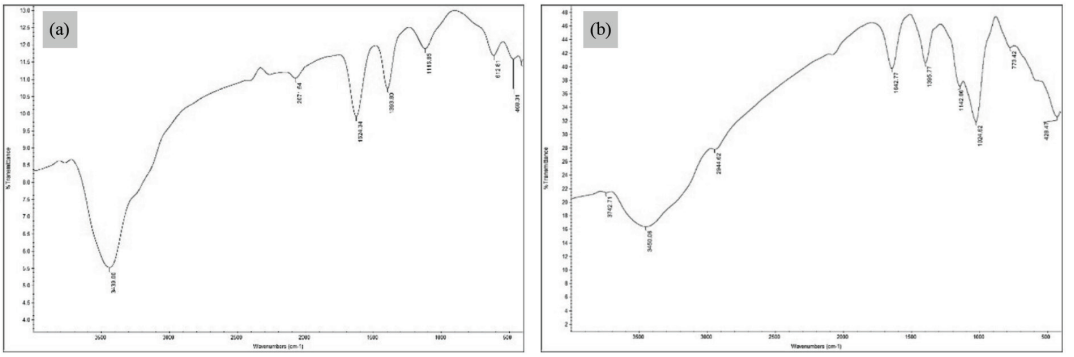


Figure 5: FTIR result for (a) raw sago hampas powder and (b) CGtO

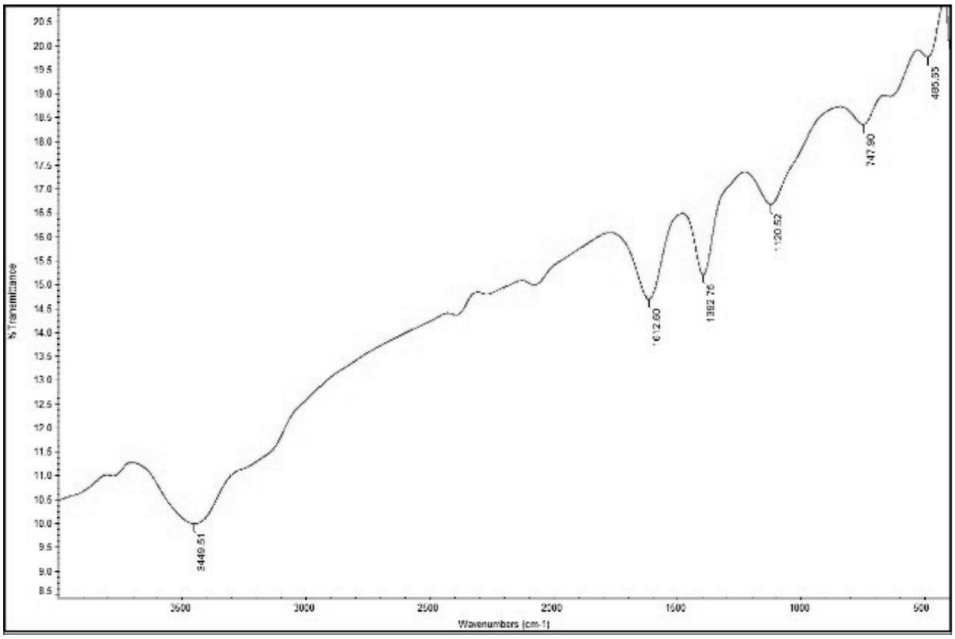


Figure 6: FTIR result of SGtO

1,117.816 cm^{-1} is assigned to the vibrations of secondary alcohols (C-OH), whereas the peak at 606.44 cm^{-1} is indicative of the vibrations of halo compounds (C-Br).

These FTIR [Figure 7 (a)] spectroscopy data confirm the presence of different oxygen-containing functional groups inside the GO structure such as hydrocarbon, hydroxyl, carboxyl, and alcohol. Surprisingly, these results are almost identical to the results of the FTIR spectrum of GO that Sujiono *et al*. reported in 2020. Variations in their chemical structures and compositions can be used to explain the little changes found in the FTIR spectra of raw sago, CGtO, SGtO, and GO [Figure 7 (b)]. Sago is a naturally occurring plant-based food that mostly contains complex carbohydrates like starch. The FTIR spectrum of carbohydrates typically highlights the characteristic vibrations and bonding of these molecules such as hydroxyl

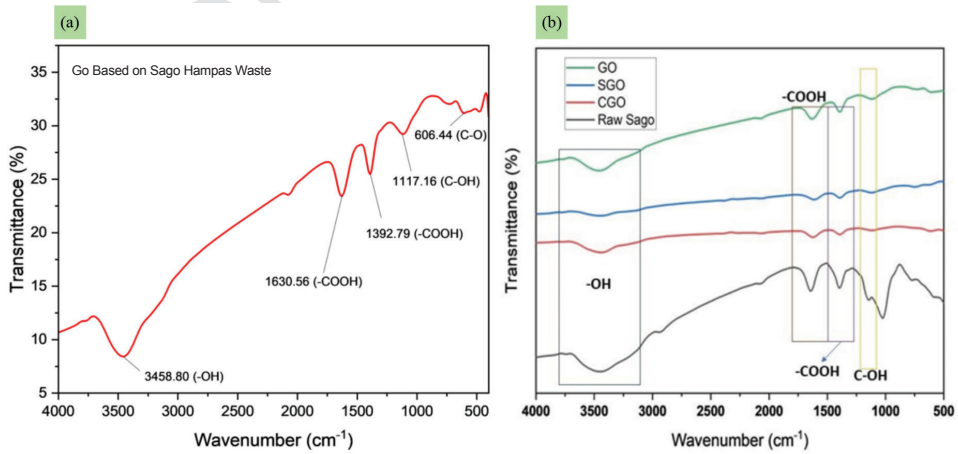


Figure 7: FTIR results of (a) GO and (b) stacked results for raw sago, CGtO, SGtO, and GO

(OH) groups and carbon-hydrogen (C-H) bonds. In contrast, CGtO, which is primarily composed of carbon arranged in highly ordered crystal structures shows a different FTIR profile. The spectrum of CGtO usually presents very few peaks or features, as carbon does not exhibit strong infrared absorption bands.

Synthetic graphite, known as SGtO is produced through a specific synthesis process that involves varying conditions and parameters. These differences can lead to alterations in the arrangement of carbon atoms and the presence of impurities or defects. Consequently, the FTIR spectra of synthetic graphite may show subtle variations from those of conventional graphite, including the appearance of new peaks or shifts in existing ones. Graphene Oxide (GO) is produced through an oxidation process that introduces oxygen-containing functional groups to the surface of graphite. These functional groups such as the carboxyl (-COOH) and hydroxyl (-OH) groups help to explain why there are unique peaks in the FTIR spectrum of GO. Depending on the synthesis technique and level of oxidation, these functional group peaks' existence and strength can change. In conclusion, differences in their chemical compositions, crystal structures, impurities, defects, and the presence of specific functional groups resulting from oxidation processes in the case of graphene oxide can explain the slight variations in the FTIR spectra of raw sago, CGtO, SGtO, and GO.

Batch Adsorption Study

Effect of pH Range on Pb(II) Adsorption

The pH impact on Pb(II) sorption is crucial, affecting both the Pb(II) species in solution and the surface properties of GO. The effect of pH on Pb(II) adsorption was examined by adjusting pH levels from 4.0 to 8.0. It can be seen based on Figure 8 that pH has a great influence on the adsorption of Pb(II) by GO. The surface characteristics of the adsorbent, qe, R, and Kd of GO on calcareous sand as a function of pH are significantly influenced by the pH of the solution (Lv *et al*., 2021). Figure 8 illustrates how all adsorption capacity and removal rates rise with rising pH at pH values greater than four. The maximum adsorption capacity and removal rate at pH 8 of Pb(II) by GO are 12.05% and 96.43%, respectively. Hence, pH 8 is the optimum pH for the adsorption of Pb(II) by GO. The data that were obtained from both equations are in Tables 4 and 5, respectively in Appendix.

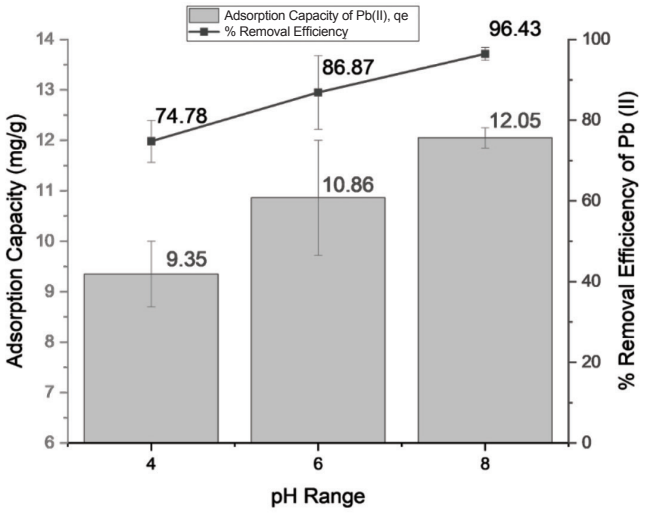


Figure 8: Adsorption capacity and percentage removal efficiency for different pH

UNCORRECTED PROOF

Effect of Pb(II) Ion Contact Time with GO

Based on Figure 9, the adsorption capacity at different contact times (hour) remains between 12.196 to 12.427 mg/g, where the optimum adsorption occurred at the first hour (12.427 mg/g). The maximum removal efficiency (99.416%) is also at the first hour of aggregation of the samples mixed GO. The removal efficiency after the first hour declined but then increased back after four hours of shaking. At four hours of shaking, there are possibilities of desorption between GO and Pb(II). Since the process is typically reversible (the opposite is called desorption), sorption is responsible for both the extraction and release of chemicals. Adsorption can happen because of chemical or physical forces, primarily because of surface energy. In general, surface particles that are partially exposed draw other particles towards them. Adsorption can be categorised in several ways depending on the type of bond (physical or chemical) created between the adsorbent and the pollutant, highlighting its features (Rápó & Tonk, 2021).

Effect of Iinitial Pb(II) Ion Concentration on Pb(II) Adsorption

Figure 10 shows that the removal efficiency is influenced by Pb(II) initial concentrations. It can be seen that as the initial concentrations of Pb(II) increase, the removal efficiency of Pb(II) on GO increases. The optimum initial concentration for the removal of Pb(II) is at 100 ppm, which removes 95% of Pb(II). The adsorption capacity of GO was able to bind to Pb(II) and reach a peak at a concentration of 20 ppm (optimum adsorption capacity – 12.5 mg/g) before declining at a concentration of 40 ppm. The adsorption capacity started to rise once more when the Pb(II) concentration was between 60 to 100 ppm, where the range of adsorption capacity is between 6.83175 to 6.8979 mg/g. The data that were obtained from both equations are shown in Tables 6 and 7, respectively in Appendix.

At first, there are many open active sites on the GO surface for Pb(II) ions to bind to at lower concentrations (up to 20 ppm). As a result, Pb(II) is removed from the solution more effectively through adsorption. The available active sites start to become saturated as the concentration rises, which lowers the adsorption effectiveness (Kaur *et al*., 2019). The active sites on the GO surface might be fully utilised or achieve their maximal capacity when the concentration hits 40 ppm. Due to the limited room for further Pb(II) ions to bind, the adsorption capacity begins to diminish. The increasing amount of Pb(II) ions in the solution, however, can cause

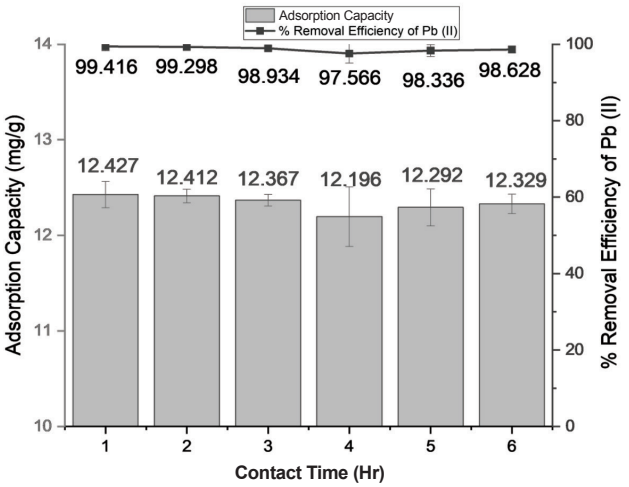


Figure 9: Adsorption capacity and percentage removal efficiency for different contact times (Hr)

Adsorption Capacity of Pb(II), qe
% Removal Efficiency

UNCORRECTED PROOF

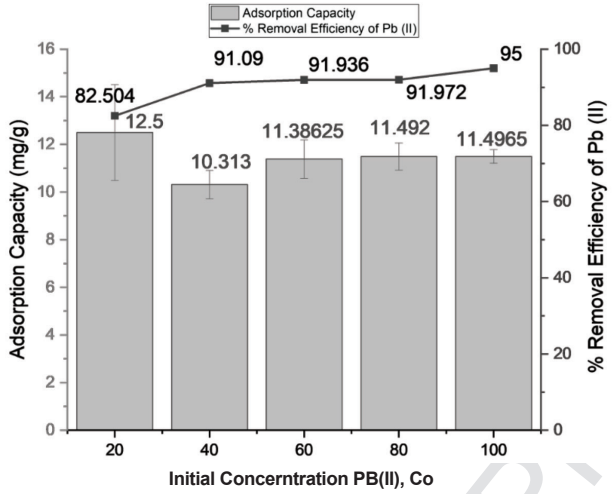


Figure 10: Adsorption capacity and percentage of removal efficiency for different initial concentrations (ppm) of Pb(II)

competition for binding sites on the GO surface when the concentration rises over 40 ppm. Due to this competition, stronger Pb(II) ions may displace weaker ones that have been adsorbed, increasing the amount of adsorption once more (Christopher *et al*., 2017).

Adsorption Isotherm

The well-known models Langmuir and Freundlich were employed in this study to ascertain the isothermal adsorption of Pb(II) on GO. Figures 11 and 12 show the adsorption isotherm models of Langmuir and Freundlich respectively. Table 1 shows the date for the isotherm parameters and the extent fitting of these regression coefficient models (R^2). Each with a consistent adsorption activation energy and enthalpy on the adsorbent surface showed a homogenous distribution of adsorption sites in the Langmuir model. Based on the data obtained in Table 1, it was found that the calculated q_{max} value is 7.032 mg/g while the K_L obtained is 7.9. The computed R^2 value obtained was 0.9588, indicating that the process of the adsorption for the Langmuir isotherm is favourable.

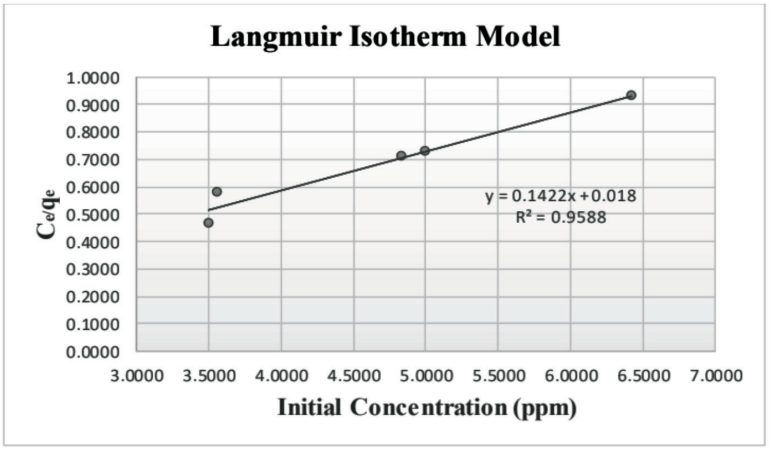


Figure 11: Graph plot of Langmuir model for Pb(II) adsorption isotherm analysis

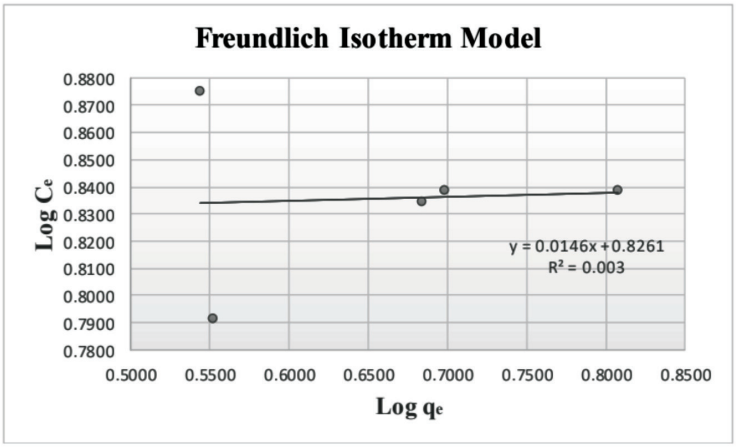


Figure 12: Graph plot of Freundlich model for Pb(II) adsorption isotherm analysis lot of Langmuir model for Pb(II) adsorption isotherm analysis

Table 1: Adsorption data analysed via Langmuir and Freundlich isotherms

Langmuir Model			Freundlich Model		
q_m	K_L	R^2	n	K_F	R^2
7.032	7.900	0.9588	68.49	6.70	0.003

In contrast, when plotting log C_e vs. log qe (Figure 13), the regression coefficient obtained is 0.003, which is not favourable compared with the Langmuir model for this adsorption study. The slope (1/n) denotes the adsorbents' surface heterogeneity or adsorption intensity. If its value approaches zero more frequently, the surface is more diverse. In this study, 1/n = 0.0146 suggests that the GO surface is less heterogeneous. But n describes the interaction that took place throughout the adsorption process. When n > 1 denotes a chemical connection, n = 1 shows no adsorption process occurs, and n < 0 denotes a physical interaction (Awang Chee *et al*., 2021). The interaction between Pb(II) and the GO in this investigation may be described as a chemisorption process because the value of n was 68.49.

Therefore, the Langmuir model is the most suitable for describing the adsorption of Pb(II) onto Graphene Oxide (GO), as evidenced by its higher R^2 value compared with other models. This suggests that the adsorption process is best represented as a monolayer coverage on a homogeneous surface, rather than a multilayer formation.

Kinetic Studies

The kinetics of Pb(II) adsorption using GO were studied using an adsorption test and analysed using the well-known kinetics isotherms models, which were the Pseudo-First-Order (PFO) and pseudo-second order (PSO). For batch kinetics of GO, plots of log (qe-qt) over the time and t/qt vs t show indicated the Pseudo-First-Order and pseudo-second order respectively. The best Pb(II) batch kinetics model was determined using the extent fitting (R^2).

Table 2 displays the Pseudo-First-Order (Figure 13) and Pseudo-Second-Order (Figure 14) kinetic data. The correlation coefficient (R2) value of 0.9999 showed that the Pseudo-Second-Order model, as opposed to the Pseudo-First-Order model (0.0187) is a superior fit for

UNCORRECTED PROOF

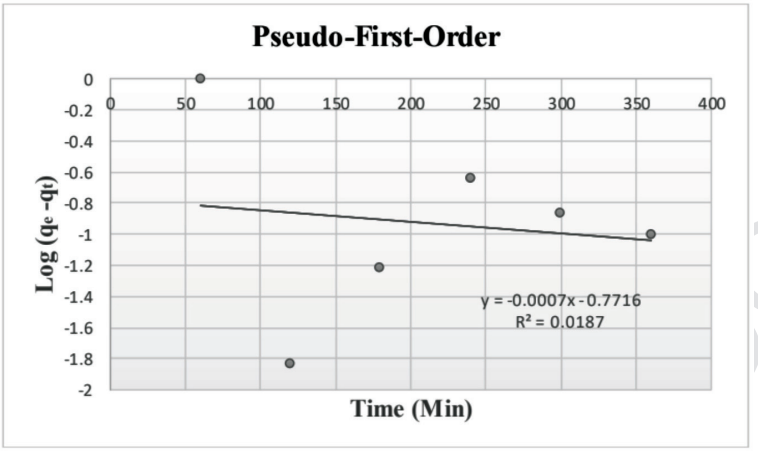


Figure 13: Graph plot of Pseudo-First-Order for kinetic studies

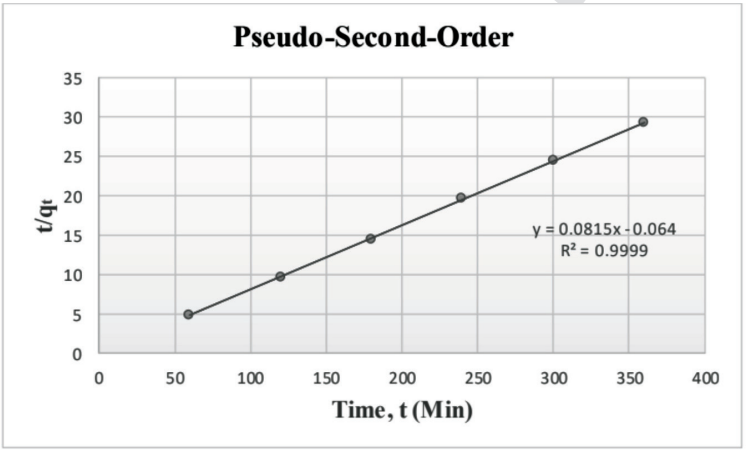


Figure 14: Graph plot of Pseudo-Second-Order for kinetic studies

Table 2: Kinetic data for Pseudo-First-Order, Pseudo-Second-Order and intra-particle diffusion

q_e (exp)	Pseudo-First-Order			Pseudo-Second-Order		
	q_e	K_1	R^2	q_e	K_2	R^2
12.4270 mg/g	0.1692 mg/g	0.0007	0.0187	12.2699 mg/g	-0.1038	0.9999

the adsorption kinetics of the GO. As a result, the Pseudo-Second-Order kinetic model is more suited and accurately describes the mechanism of Pb(II) adsorption to the GO. Furthermore, the experimental value and the theoretical value of qe from the Pseudo-Second-Order model. In this model, the surface adsorption step, involving chemisorption and the removal of Pb(II) from the solution through physicochemical interactions between the phases is identified as the rate-limiting step. Consequently, the adsorption study for Pb(II) removal demonstrates that the Pseudo-Second-Order model provides a superior fit, highlighting that the adsorption process is primarily chemical in nature were nearly identical.

Table 3: Previously reported studies related to Pb(II) removal with different adsorbents

Type of Adsorbents	Type of Treatments	OptimumF Parameters	Adsorption Capacity (mg/g)	Removal Efficiency (%)	Fitted Adsorption and Kinetics Isotherms	References
Graphene Oxide (GO)	Membrane separation	pH: 5	255	Not mentioned	Not related	(Nguyen *et al.*, 2021)
2-acetylthiophene-modified graphene oxide (A-GO)	Adsorption	Not mentioned	408	Not mentioned	Langmuir Pseudo-Second-Order (PSO)	(Guo *et al.*, 2022)
GO reduction by green tea extraction	Biogenic method	pH: 8 Dose: 10 $g \cdot L^{-1}$ Temperature: 80°C	Not mentioned	97.2	Not related	(Weng *et al.*, 2019)
Zinc oxide/graphene oxide Nanocomposites (ZnO/GO)	Adsorption	pH: 5 Adsorbent dosage: 0.16 mg/L Optimum time: 160 minutes	418.78	Not mentioned	Pseudo-First-Order (PFO)	(Ahmad *et al.*, 2020)
GO-MIL-53(Al) nanocomposites	Adsorption	pH: 11 Adsorbent dosage: 2 g/L Initial concentration: 90 mg/L Contact time: <30 minutes	232	Not mentioned	Langmuir Pseudo-Second-Order	(Chowdhury *et al.*, 2021)
Graphene Oxide (GO) from sago hampas waste	Adsorption	pH: 8 Initial concentration: 100 ppm Optimum time: 60 minutes	11.5	95	Langmuir Pseudo-Second-Order (PSO)	Present study

UNCORRECTED PROOF

A comparison of the percentage of Pb(II) removal and the adsorption capacity of different GO-containing adsorbents is presented in Table 3. Although the adsorption capacity of the GO synthesised in this study is the lowest, the adsorbent is capable of removing up to 95% of Pb(II) ions. In terms of the adsorption mechanism, the results obtained in this study are consistent with those reported in previous studies.

Conclusions

Graphene Oxide (GO) was successfully synthesised from sago waste hampas using a modified Hummers method. FTIR spectroscopy confirmed the presence of various oxygen-containing functional groups such as hydroxyl, carboxyl, alcohol, and epoxy, indicating that the GO structure was successfully formed. Additionally, the surface morphology analysis of the GO sample revealed granular particles with a range of sizes, showcasing its distinctive characteristics. Moreover, batch adsorption studies revealed that the optimal pH for Pb(II) adsorption onto GO is pH 8, with the adsorption process occurring within the first hour. GO achieved the highest removal efficiency for Pb(II) ions from an initial concentration of 100 ppm. The adsorption process was best described by the Langmuir isotherm model and the pseudo-second-order kinetic model, indicating monolayer adsorption on a homogeneous surface and a physisorption mechanism.

However, further research is needed to evaluate the efficiency of Pb(II) removal by Graphene Oxide (GO) more comprehensively. This includes optimising GO production from sago waste hampas to improve its effectiveness in adsorbing Pb(II) during water treatment. Future studies should also investigate additional parameters, such as adsorbent dosage and temperature to enhance the yield and quality of the adsorbent. Additionally, scaling up these tests to industrial levels should be considered to refine the quality of GO for removing Pb(II) and other metals. These recommendations aim to advance GO production from the sago hampas and its effectiveness in heavy metal removal during water treatment. In conclusion, the batch adsorption process using GO demonstrated rapid Pb(II) ion removal, highlighting its potential as a sustainable solution for future wastewater management practices.

Acknowledgements

This work was financially funded by the Shell Chair (UNI/F07/SHC/85529/2023) and the Research Grant Award (UNI/F07/RISE/85739/2023) from Universiti Malaysia Sarawak.

Conflict of Interest Statement

The authors declare that they have no conflict of interest.

References

Ahmad, S. Z. N., Salleh, W. N. W., Yusof, N., Yusop, M. Z. M., Hamdan, R., Awang, N. A., Ismail, N. H., Rosman, N., Ibrahim, H., & Ismail, A. F. (2020). Efficient removal of Pb(II) from aqueous solution using zinc oxide/graphene oxide composite. *IOP Conference Series: Materials Science and Engineering*, *736*(5). https://doi.org/10.1088/1757-899X/736/5/052002

Amin, N. M, Sabli, N., Izhar, S., & Yoshida, H. (2019). A review: Sago wastes and its applications. *Pertanika Journal of Science and Technology*, *27*, 1841-1862. https://www.researchgate.net/publication/339499340_A_review_Sago_Wastes_and_Its_Applications

Awang Chee, D. N., Aziz, F., Mohamed Amin, M. A., & Ismail, A. F. (2021). Copper adsorption on ZIF-8/Alumina hollow fiber membrane: A response surface methodology analysis. *Arabian Journal for Science and Engineering*, *46*(7), 6775-6786. https://doi.org/10.1007/s13369-021-05636-1

Balali-Mood, M., Kobra, N., Zoya, T., Reza, K. M., & Mahmood, S. (2021). Toxic

UNCORRECTED PROOF

mechanisms of five heavy metals: Mercury, lead, chromium, cadmium, and arsenic. *Frontiers in Pharmacology*, *12*. https://www.frontiersin.org/articles/10.3389/fphar.2021.643972

Bohari, N., Mohidin, H., Idris, J., Ando, Y., Man, S., Saidan, H., & Suraiya, M. (2020). Nutritional characteristics of biochar from pineapple leaf residue and sago waste. *Pertanika Journal of Science and Technology*, *28*, 273-286. DOI: 10.47836/pjst 28. S2.21.

Chaudhry, F. N., & Malik, M. F. (2017). Factors affecting water pollution: A review. *Journal of Ecosystem & Ecography*, *07*(01). DOI: 10.41722157-7625.1000225.

Chowdhury, T., Zhang, L., Zhang, J., & Aggarwal, S. (2021). Pb(ii) adsorption from aqueous solution by an aluminum-based metal organic framework-graphene oxide nanocomposite. *Materials Advances*, *2*(9). https://doi.org/10.1039/d1ma00046b

Christopher, F. C., Anbalagan, S., Kumar, P. S., Pannerselvam, S. R., & Vaidyanathan, V. K. (2017). Surface adsorption of poisonous Pb(II) ions from water using chitosan functionalised magnetic nanoparticles. *IET Nanobiotechnology*, *11*(4), 433-442. https://doi.org/10.1049/iet-nbt.2016.0166

Guo, Y., Wu, D. F., Wu, H. M., Liu, X. Y., Xu, H. Z., & Chen, Q. Q. (2022). Efficient removal of Pb(II) ions by using 2-acetylthiophene-modified graphene oxide from aqueous solution. *Materials Today Sustainability*, *20*, 100212. https://doi.org/10.1016/J.MTSUST.2022.100212

Kaur, M., Kumari, S., & Sharma, P. (2019). Removal of Pb(II) from aqueous solution using nanoadsorbent of Oryza sativa husk: Isotherm, kinetic and thermodynamic studies. *Biotechnology Reports (Amsterdam*, *Netherlands)*, *25*, e00410. https://doi.org/10.1016/j.btre.2019.e00410

Khurana, I., Shaw, A. K., Bharti, Khurana, J. M., & Rai, P. K. (2018). Batch and dynamic adsorption of Eriochrome Black T from water on magnetic graphene oxide: Experimental and theoretical studies. *Journal of Environmental Chemical Engineering*, *6*(1), 468-477. DOI: 10.1016/j.jece.2017.12.029.

Lv, B., Yu, W., Luo, J., Qian, B., Asefa, M. B., & Li, N. (2021). Study on the adsorption mechanism of graphene oxide by calcareous sand in South China Sea. *Adsorption Science & Technology*, *2021*, Article ID 2227570, 15 pages. https://doi.org/10.1155/2021/2227570

Nguyen, M. T., Zhang, J., Prabhakaran, V., Tan, S., Baxter, E. T., Shutthanandan, V., Johnson, G. E., Rousseau, R., & Glezakou, V. A. (2021). Graphene oxide as a Pb(II) separation medium: Has part of the story been overlooked? *JACS Au*, *1*(6). https://doi.org/10.1021/jacsau.0c00075

Qasem, N. A. A., Mohammed, R. H., & Lawal, D. U. (2021). Removal of heavy metal ions from wastewater: A comprehensive and critical review. *NPJ Clean Water*, *4*, 36. https://doi.org/10.1038/s41545-021-00127-0

Rápó, E., & Tonk, S. (2021). Factors affecting synthetic dye adsorption; Desorption studies: A review of results from the last five years (2017-2021). *Molecules (Basel*, *Switzerland)*, *26*(17), 5419. https://doi.org/10.3390/molecules26175419

Shojaeenezhad, S., Farbod, M., & Iraj, K. (2017). Effect of initial graphite particle size and shape on oxidation time in graphene oxide prepared by Hummers' method. *Journal of Science: Advanced Materials and Devices*, *2*. DOI: 10.1016/j.jsamd.2017.09.003.

Sujiono, E. H., Zurnansyah, Zabrian, D., Dahlan, M. Y., Amin, B. D., Samnur, & Agus, J. (2020). Graphene oxide-based coconut shell waste: Synthesis by modified Hummer's method and characterization. *Heliyon*, *6*(8), e04568. https://doi.org/10.1016/j.heliyon2020.e04568

UNCORRECTED PROOF

United Nations. (2018). *Sustainable Development Goal 6: Synthesis Report on Water and Sanitation*. https://sustainabledevelopment.un.org/content/documents/19901SDG6_SR2018_web_3.pdf

Weng, X., Wu, J., Ma, L., Owens, G., & Chen, Z. (2019). Impact of synthesis conditions on Pb(II) removal efficiency from aqueous solution by green tea extract reduced graphene oxide. *Chemical Engineering Journal*, *359*. https://doi.org/10.1016/j.cej.2018.11.089

Yu, H., Zhang, B., Bulin, C., Li, R., & Xing, R. (2016). High-efficient synthesis of graphene oxide based on Improved Hummers Method. *Scientific Reports*, *6*(1). https://doi.org/10.1038/srep3614

UNCORRECTED PROOF

Appendix

Table 4: Percentage of removal efficiency and standard deviation for the average concentration of Pb(II) at different pH ranges

pH Range	Percentage of Removal Efficiency of Pb(II)	Standard Deviation
4	74.79	5.2089
6	86.87	9.1078
8	96.43	1.5842

Table 5: Adsorption capacity and standard deviation for the average concentration of Pb(II) at different pH ranges

pH Range	Adsorption capacity of Pb(II)	Standard Deviation
4	9.35	0.6511
6	10.86	1.1385
8	12.05	0.198

Table 6: Percentage of removal efficiency and standard deviation for the average concentration of Pb(II) at different initial concentrations

Initial Concentration Pb(II), Co	Percentage of Removal Efficiency of Pb(II)	Standard Deviation
100	95	2.286
80	91.972	4.59
60	91.936	6.426
40	91.09	4.789
20	82.504	16.073

Table 7: Adsorption capacity and standard deviation for the average concentration of Pb(II) at different initial concentrations

Initial Concentration Pb(II), Co	Adsorption Capacity	Standard Deviation
100	6.8979	0.2858
80	6.8952	0.5738
60	6.83175	0.8033
40	6.1878	0.5987
20	7.5	2.0092

UNCORRECTED PROOF